Light–Assisted Synthesis of Metal Oxide Heirarchical Structures and Their Catalytic Applications

8 AUTHORS, INCLUDING:

Aparna Iyer
University of Connecticut
7 PUBLICATIONS **157** CITATIONS

SEE PROFILE

Naftali Opembe
Ames Laboratory of the US DOE
17 PUBLICATIONS **276** CITATIONS

SEE PROFILE

Hui Huang
University of Connecticut
22 PUBLICATIONS **804** CITATIONS

SEE PROFILE

Steven L Suib
University of Connecticut
652 PUBLICATIONS **15,529** CITATIONS

SEE PROFILE

Light-Assisted Synthesis of Metal Oxide Heirarchical Structures and Their Catalytic Applications

Cecil K. King'ondu,[§] Aparna Iyer,[§] Eric C. Njagi,[§] Naftali Opembe,[§] Homer Genuino,[§] Hui Huang,[§] Roger A. Ristau,[†] and Steven L. Suib*[,§,†]

[§]Department of Chemistry and [†]Institute of Materials Science, University of Connecticut, Storrs, Connecticut 06269, United States

S *Supporting Information*

ABSTRACT: Short reaction times and morphology control in the synthesis of inorganic materials under nonthermal conditions remain a challenge. Herein we report a rapid, self-templating, and nonthermal method based on ultraviolet light to prepare metal oxide hierarchical structures. With this method, the morphology of the metal oxides was controlled readily without using templates.

Nanoscale inorganic materials with one-, two-, and three-dimensional order have drawn much attention due to the size/shape—property correlation that has been revealed by nanotechnology over the past 20 years. Recently, the power conversion efficiency in a bulk heterojunction solar cell has been shown to depend strongly on the morphology of the photoactive C_{60} layer.[1] This correlation has engendered the need for synthetic strategies where particle size and morphology can be precisely controlled routinely to prepare materials with enhanced functionalities in gas sensing,[2] separation,[3] energy storage,[4] coating, data storage,[5] catalysis,[6] and bio-diagnostic sensing.[7]

Currently, inorganic nanomaterials are synthesized by top-down approaches, in which bulk materials are reduced to nanoscale particles. Additionally, bottom-up approaches are used where inorganic nanomaterials are constructed from the basic units (atoms or molecules) via a chemical reaction. In the bottom-up approach, particle size is tailored by controlling the rate at which and/or the extent to which crystals grow. This is done by use of co-solvents[8] and manipulation of temperature, pressure, pH, and time. Shape, on the other hand, is tailored by controlling the assembly of the secondary building blocks. Most of the current bottom-up approaches entail suppling heat energy to or creating heat energy within the reaction mixture, as is the case with conventional oil-bath and microwave methods, respectively. Moreover, templates, structure-directing agents, and surfactants, such as silica,[9] polymethyl methacrylate,[10] ethylene glycol,[11] and dodecylamine,[12] are often used to control the morphology and porosity of metal oxides. By use of dodecylamine,[12] mesoporous molybdenum and niobium oxides have been synthesized.

Herein, we present a rapid, self-templating, and nonthermal approach based on ultraviolet (UV) light for synthesizing γ-manganese oxide (γ-MnO$_2$), cobalt oxide hydroxide (CoOOH), and cerium oxide (CeO$_2$) hierarchical nanoarchitectures. The use of UV light to prepare crystalline metal oxide nanostructures has not been reported. The novelty of our present study therefore lies in the use of UV light to prepare crystalline metal oxides. The shape, surface area, and porosity of these materials can be precisely tailored without the use of templates or structure-directing agents. The ability to attain short reaction times (8 min) under nonthermal conditions, as opposed to conventional oil-bath and microwave heating, is also unique. To eliminate thermal effects and maintain constant low temperatures, the quartz reactor used was jacketed with ice or flowing water (see Supporting Information (SI), Figure S1).

The light-mediated synthetic method presented herein is premised on coupled photolysis and acid-catalyzed decomposition of aqueous persulfate ions ($S_2O_8{}^{2-}$) to generate very powerful oxidizing sulfate radicals (2.5—3.1 V).[13] These radicals ($SO_4{}^{\bullet-}$) then oxidize Mn^{2+}, Co^{2+}, and Ce^{3+} ions in respective reaction mixtures to γ-MnO$_2$, CoOOH, and CeO$_2$.

Morphological studies conducted by field emission scanning electron microscopy (FESEM) show that the as-synthesized γ-MnO$_2$ material consists of microspheres with average diameters ranging from 0.5 to 2.0 μm (Figure 1a). Further structural studies done with high-resolution transmission electron microscopy (HRTEM) show that the γ-MnO$_2$ microspheres synthesized for 30 and 60 min were hollow. This is evident from the annular structure shown in Figure 1b, where the dark ring and the light inner regions represent the porous shell and the empty core of the microsphere, respectively. The porous shell is made up of the γ-MnO$_2$ nanofibers (Figure 1c) that are structurally single crystalline, as shown by the periodic lattice fringes of 2.8 Å corresponding to the (021) planes (Figure 1c, inset).

To gain insight into the formation mechanism of the hollow γ-MnO$_2$ microspheres observed with HRTEM, time-dependent studies were performed. Samples were taken periodically by means of a syringe and their morphologies studied by FESEM, HRTEM, and focused ion beam (FIB). The sample taken after 2 min of irradiation shows microspheres with fairly smooth surfaces (SI, Figure S2a). After 4 min, the microspheres became relatively rough, indicating that the MnO$_2$ crystallites on the surface of the microspheres had started growing into large particles (Figure S2b). After 6 min, pseudo-fibers started to appear on the surfaces of the microspheres (Figure S2c). As the time progressed to 8, 10, 15, and 30 min, well-developed microspheres with fibrous surfaces formed (Figure S2d,e and Figure 1i, j, respectively). Upon slicing through the microspheres synthesized for 4, 6, 8, 10, and 15 min using FIB, solid cores with pores
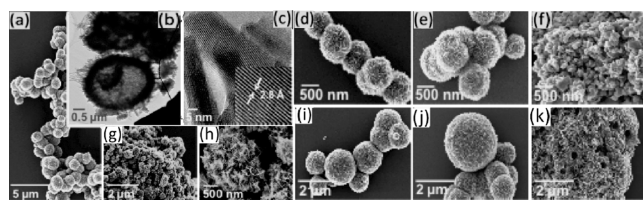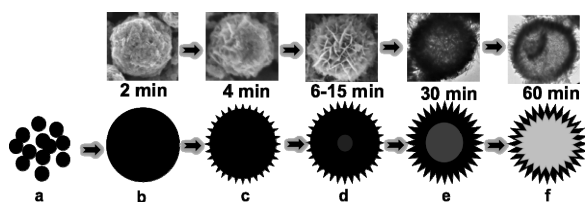
Figure 1. (a) FESEM image showing the general morphology of γ-MnO$_2$. (b) HRTEM image showing the hollow core—porous shell. (c) γ-MnO$_2$ nanofibers. The inset shows magnified (021) lattice fringes. (d–f) γ-MnO$_2$ synthesized at 30–33, 22–23, and 8–10 °C, respectively. (g,h) γ-MnO$_2$ synthesized for 30 min without nitric acid. (i–k) γ-MnO$_2$ synthesized for 15, 30, and 60 min, in that order.

Figure 2. FESEM images showing the microsphere morphology of (a–c) CeO$_2$ synthesized for 15, 30, and 60 min, respectively; (d) CeO$_2$ synthesized for 30 min without acid; (e,f) CoOOH synthesized for 60 and 120 min, respectively. The bottom-left inset in panel f shows a magnified (1 μm) image of a CoOOH flower. The bottom-right inset in panel f shows the flakes that make up the CoOOH flowers.

Scheme 1. Formation of the Solid and Hollow Core—Porous Shell γ-MnO$_2$ Microspheres

Scheme 2. Formation of the Solid CeO$_2$ Microspheres

were observed (SI, Figure S3), in contrast to the hollow cores observed by HRTEM in microspheres prepared for 30 min (Figure 1b).

On the basis of the time dependence, it is suggested that the generated SO$_4^{\bullet-}$ radicals oxidized Mn^{2+} ions in the reaction mixture to MnO$_2$ nucleating species/crystallites (Scheme 1a). The crystallites then self-assembled into microspheres under the influence of interfacial/surface forces[14] (Scheme 1b).

After the self-assembly of the initial crystallites (which formed rapidly due to the initial high supersaturation conditions[15]) into microspheres, the crystallites on or near the surface of the microspheres continued to grow slowly due to the low supersaturation conditions created after the primary nucleation. Consequent to this growth, relatively large crystals formed on the surface of the microspheres (Scheme 1c), and this set up a concentric crystallite size gradient where the large crystals resided on the surface of the microspheres and the smaller ones in the cores.

Due to the high surface energy of the smaller crystallites compared to the larger ones, the smaller crystallites in the cores dissolved and re-crystallized on larger ones. The onset of this dissolution and re-deposition process (generally referred to as the Ostwald ripening process[16,17]) is shown in Scheme 1d. With time, the concentric crystallite size gradient allowed for symmetric hollowing (Scheme 1e), and this gave rise to the observed hollow core—porous shell microspheres (Figure 1b). Reaction time and temperature control are thus critical in realization of hollow core—shell morphologies.

With the UV light synthetic strategy we developed, the morphology of the γ-MnO$_2$ material could be controlled readily and precisely by simply varying the temperature, the UV light intensity, the irradiation time, and the pH of the reaction mixture (see discussion in the SI on how temperature, UV intensity, irradiation time, and pH were varied). In the 32–33 °C temperature range, microspheres were formed (Figure 1d). When the temperature was lowered to 22–23 °C, microspheres were
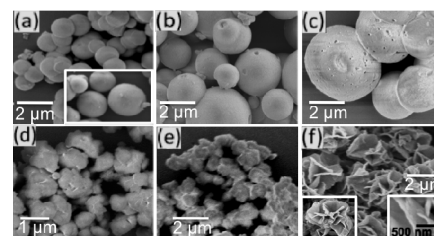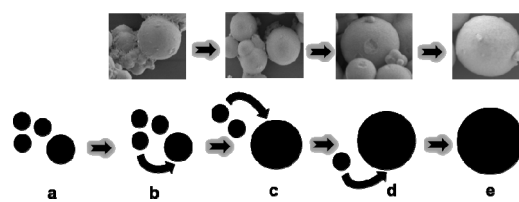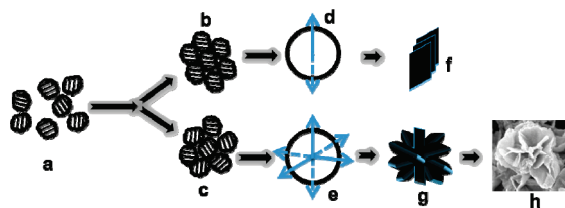
still obtained (Figure 1e). However, on further reducing the temperature to 8–10 °C, no microspheres formed (Figure 1f). Changing the pH of the reaction mixture by omitting nitric acid from the γ-MnO$_2$ recipe led to aggregates of flake-like particles instead of microspheres (Figure 1g,h). Upon reducing the UV intensity by reducing the number of UV lamps, poorly formed microspheres with amorphous-like surfaces were obtained (SI, Figure S4).

Omission of nitric acid and reduction of the UV light intensity decreased the rate of decay of S$_2$O$_8^{2-}$ ions. This, in turn, reduced the amount of SO$_4^{\bullet-}$ radicals (the oxidant) generated and led to inadequate oxidation of Mn^{2+} ions in the reaction mixture. Acidic media and UV light intensity are thus crucial in controlling the rate of decay of S$_2$O$_8^{2-}$ ions and hence the morphology.

On the other hand, increasing the irradiation time from 15 to 30 min afforded well-developed microspheres (Figure 1i,j). However, increasing the irradiation time to 60 min destroyed the microspherical structure, leading to the creation of open cavities (Figure 1k). The observed destruction corroborates the proposed Ostwald ripening process in that, at 60 min, symmetric hollowing translated to very thin and weak porous shells, so weak so that the hollow microspheres collapsed.

Likewise, varying the pH and irradiation time controlled the morphology of CeO$_2$ and CoOOH materials. CeO$_2$ materials synthesized for 15, 30, and 60 min with acid showed a homogeneous morphology composed of microspheres with average diameters of about 500 nm (Figure 2a–c). When a slice was cut through a few of these microspheres by FIB, no hollow cores were observed (SI, Figure S5), indicating that the microspheres were not hollow. Unlike γ-MnO$_2$ materials, CeO$_2$ maintained microspherical morphology at 60 min of irradiation. Similar to γ-MnO$_2$ materials (Figure 1d,e), no CeO$_2$ microspheres were obtained when nitric acid was omitted (Figure 2d). On the other hand, no solid CoOOH materials formed in the presence of the acid. Nonetheless, without the acid, amorphous CoOOH materials

Scheme 3. Formation of the CoOOH Flowers

Figure 3. (a) XRD patterns of γ-MnO_2, CeO_2, and CoOOH materials synthesized for 15, 15, and 120 min, respectively. (b) N_2 adsorption/desorption isotherms for γ-MnO_2 materials synthesized for 15, 30, and 60 min. Insets show interstices between microspheres.

were obtained after 60 min of irradiation (Figure 2e). Upon increasing the irradiation time to 90 and 120 min, CoOOH materials with flower-like morphology were obtained (Figure 2f).

The solid CeO_2 microspheres are formed as shown in Scheme 2. First, CeO_2 nucleating species/crystallites resulting from the oxidation of Ce^{3+} ions by $SO_4^{\bullet-}$ radicals self-assembled into spherical aggregates of unequal sizes (Scheme 2a). With time, the smaller and thermodynamically unfavored spherical aggregates successively coalesced onto the larger ones, thereby giving rise to large microspheres (Scheme 2b−d).

Since the microspheres apparently formed by deposition of the smaller aggregates onto larger ones, no gradient in terms of crystallite size was set up in the resultant microspheres. As such, symmetric or asymmetric hollowing by an Ostwald ripening process could not take place, and this led to solid CeO_2 microspheres. The proposed mechanism is affirmed by the fact that the resultant CeO_2 microspheres, just like the initial aggregates, are of different sizes (SI, Figure S6a), in contrast to the γ-MnO_2 microspheres that seem equal in their sizes (Figure S6b). The aggregation of crystallites and agglomeration into large microspheres is probably mediated by sulfate ions (SO_4^{2-}). Sulfate ions have been reported to mediate agglomeration and formation of globular CeO_2 particles[18] and boehmite microspheres.[19] In addition, attenuated total reflectance (ATR) data (SI, Figure S7) show a broad absorption band at 960−1180 cm^{-1} that, based on the work of Xu et al.,[20] corresponds to SO_4^{2-} ions adsorbed on Ce^{4+} surface cations of our CeO_2 material.

The CoOOH flowers, on the other hand, are suggested to form via a three-step mechanism shown in Scheme 3. The first step was nucleation and formation of CoOOH nanocrystals (Scheme 3a). The nanocrystals then self-assembled into pseudo-flower aggregates similar to the ones shown in Figure 2e. Within the respective aggregates, the nanocrystals rearranged to attain similar crystallographic orientation (Scheme 3b) and thus lower the energy of the system.[21,22] However, since nanocrystal surfaces are not atomically flat, crystallographic disorientation due to curvature in the adjoining nanocrystals often occurs (Scheme 3c).

After the self-assembly and rearrangement, the nanocrystals underwent an oriented attachment growth process where smaller crystallites attached to each other along the same crystallographic direction.[16,23] Due to the layered crystal lattice of CoOOH[24] and the restriction of the oriented attachment (OA) growth to one preferred crystallographic direction,[22] the growth of these nanocrystals in the aggregates led to the formation of one-dimensional CoOOH flakes. Formation of nanoflakes has also been observed in other layered materials, for instance boehmite.[19] Because the initial CoOOH nanocrystals in the aggregates were presumed to be disoriented (Scheme 3c), OA occurred in different directions, as shown in Scheme 3e. This therefore led to the formation of CoOOH flakes fused at one end and branching out at the other ends to form flowers (Scheme 3g,h).
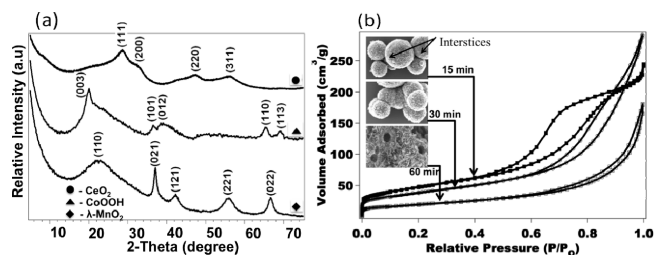
X-ray diffraction (XRD) data (Figure 3a) confirmed that the as-synthesized γ-MnO_2, CoOOH, and CeO_2 materials were crystalline. Elemental analyses of energy-dispersive X-ray absorption spectroscopy (EDAX) data (SI, Figure S8) show trace amounts of potassium and sulfur in γ-MnO_2 and CoOOH materials, an indication that neither K^+ nor SO_4^{2-} ions were incorporated into their structure. This in part led to the suggestion that $SO_4^{\bullet-}$ radicals are not involved in the γ-MnO_2 and CoOOH crystal growth but trigger nucleation. Quite opposite of γ-MnO_2 and CoOOH materials, a substantial amount of sulfur was detected in CeO_2 materials, even after washing several times. The detected sulfur was probably due to the sulfate ions adsorbed on the Ce^{4+} cations.[18] Determination of the adsorption/binding mode(s) of SO_4^{2-} ions to CeO_2 materials, investigation of ways to reduce the adsorption, and unequivocal confirmation of the role played by this binding in the CeO_2 crystal growth and morphology evolution are being pursued in our continuing studies.

In addition to facile morphology control offered by our new method, the textural properties of the γ-MnO_2 material can be tailored more easily and precisely by just varying the irradiation time. The BET surface area decreased dramatically from 179 to 71 m^2/g when time was increased from 15 to 60 min. Similarly, mesoporosity of the γ-MnO_2 material decreased markedly upon increasing the time to 60 min. This is evident from the shift of the N_2 adsorption/desorption isotherms from type-IV (quintessential for corpuscular systems[25]) to type-II (typical for fibrous particles[26]) (Figure 3b).

Moreover, the H_2-type hysteresis loop observed for γ-MnO_2 material synthesized at 15 min decreased upon increasing the irradiation time to 30 min and transformed to an H_3-type hysteresis loop (typical for slit-shaped mesopores[27]) at 60 min (Figure 3b). The pore size distribution, on the other hand, increased significantly from 7 to 14 nm when the irradiation time was increased from 15 to 60 min (SI, Table S1). The high mesoporosity of the γ-MnO_2 material synthesized for 15 min is suggested to arise from the pores inside the microspheres (SI, Figure S3d) and the interstitial spaces between adjoining microspheres (Figure 3b, top-inset). Therefore, the decrease in the H_2-type hysteresis loop size after 30 min of irradiation was probably due to the loss of interstitial pores between adjacent microspheres caused by coalescence of the microspheres (Figure 3b, middle-inset). The transformation of the H_2-type hysteresis loop to H_3-type at 60 min was due to the destruction of the microsphere morphology, leading to formation of open holes and partly segregated nanofibers (Figure 3b, bottom-inset).

The role played by UV light in our syntheses was investigated by carrying out a set of experiments for each material (γ-MnO_2, CoOOH, and CeO_2), where one experiment was conducted with

UV light and the other without. A representative set of experiments on γ-MnO$_2$ (SI, Figure S9) shows that after 3 min of UV light irradiation, the reaction mixture changed from clear to light brown, suggesting MnO$_2$ nucleation. In contrast, the reaction mixture remained clear even after 5 h of stirring with the UV light off. Upon replacing the UV lamps with the same number of visible lamps ($\lambda = 700-400$ nm), no γ-MnO$_2$, CoOOH, and CeO$_2$ materials were formed, implying that UV light played a significant role in our syntheses.

The catalytic activity of the γ-MnO$_2$ and CoOOH materials was tested for oxidation of 4-biphenylmethanol with *tert*-butyl hydroperoxide as the oxidant (SI, Table S2). CoOOH and γ-MnO$_2$ have been used as catalysts in selective oxidation of cumene,[28] cinnamyl,[29] and benzyl alcohol.[30] The γ-MnO$_2$ microspheres synthesized for 15 min showed the highest conversion of 91%, with selectivity of 84% toward 4-phenylbenzaldehyde. In contrast, as-synthesized CoOOH showed the lowest conversion (58%) and the highest selectivity (96%). The conversions obtained at much shorter reaction time (30 min) using cheaper catalysts are comparable to similar substrate oxidation procedures in the liquid phase with carbon-supported platinum and Mo−V−O-based catalysts.[31−33]

In conclusion, we have successfully demonstrated a rapid, self-templating, and nonthermal approach for synthesizing crystalline, hierarchical γ-MnO$_2$, CeO$_2$, and CoOOH nanostructures under UV light at temperatures as low as 8−10 °C and reaction times as short as 8 min. The technique presented herein sets forth a new avenue through which crystalline metal oxide nanostructures can be prepared and their morphology controlled through a nonthermal method. We have preliminary data on synthesis of OMS-2 and ZnO, and the technique is currently being extended to the synthesis of other metal oxide nanomaterials, such as TiO$_2$ and Cr$_2$O$_3$, as part of our continuing research.

■ ASSOCIATED CONTENT

ⓢ Supporting Information. Experimental procedure, Figures S1−S9, and Tables S1 and S2. This material is available free of charge via the Internet at http://pubs.acs.org.

■ AUTHOR INFORMATION

Corresponding Author
steven.suib@uconn.edu

■ ACKNOWLEDGMENT

■ REFERENCES

(1) Peet, J.; Senatore, M. L.; Heeger, A. J.; Bazan, G. C. *Adv. Mater.* **2009**, *21*, 1521–1527.

(2) Geng, B.; Zhan, F.; Jiang, H.; Xing, Z.; Fang, C. *Cryst. Growth Des.* **2008**, *8*, 3497–3500.

(3) Masamichi, T. *Solvent Extr. Ion Exch.* **2001**, *19*, 531–551.

(4) Euler, K. J.; Mueller-Helsa, H. *J. Power Sources* **1979**, *4*, 77–89.

(5) Huaqiang, C.; Guozhi, W.; Lei, Z.; Yu, L.; Sichun, Z.; Xinrong, Z. *ChemPhysChem* **2006**, *7*, 1897–1901.

(6) Sithambaram, S.; Kumar, R.; Son, Y.-C.; Suib, S. L. *J. Catal.* **2008**, *253*, 269–277.

(7) Robert, W. *Chem. Soc. Rev.* **2008**, *37*, 2028.

(8) Nyutu, E. K.; Chen, C.-H.; Sithambaram, S.; Crisostomo, V. M. B.; Suib, S. L. *J. Phys. Chem. C* **2008**, *112*, 6786–6793.

(9) Yoshiyuki, K.; Kazuyuki, K. *Angew. Chem. Int. Ed.* **2010**, *49*, 6993–6997.

(10) Masahiro, S.; Toshitaka, H.; Nobuyasu, K.; Keisuke., S.; Wataru, U. *J. Solid State Chem.* **2010**, *183*, 1365–1371.

(11) Fangyi, C.; Jun, C.; Xinglong, G.; Panwen, S. *Adv. Mater.* **2005**, *17*, 2753–2756.

(12) (a) Antonelli, D. M.; Trudeau, M. *Angew. Chem. Int. Ed.* **1999**, *38*, 1471–1475. (b) Rao, Y.; Trudeau, M.; Antonelli, D. *J. Am. Chem. Soc.* **2006**, *128*, 13996–13997.

(13) (a) Dogliotti, L.; Hayon, E. *J. Phys. Chem.* **1967**, *71*, 2511. (b) House, D. A. *Chem. Rev.* **1962**, *62*, 185.

(14) Yuan, J.; Laubernds, K.; Zhang, Q.; Suib, S. L. *J. Am. Chem. Soc.* **2003**, *125*, 4966–4967.

(15) Liu, B.; Zeng, H. C. *Small* **2005**, *1*, 566–571.

(16) Zeng, H. C. *Curr. Nanosci.* **2007**, *3*, 177–181.

(17) Lei, J.; Xu, L.; Morein, C.; Chen, C.-H.; Lai, M.; Dharmarathna, S.; Dobley, A.; Suib, S. L. *Adv. Funct. Mater.* **2010**, *22*, 3373.

(18) Hirano, M.; Fukuda, Y.; Iwata, H.; Hotta, Y.; Inagaki, M. *J. Am. Ceram. Soc.* **2000**, *83*, 1287–1289.

(19) Cai, W.; Yu, J.; Gu, S.; Jaroniec, M. *Cryst. Growth Des.* **2010**, *10*, 3977–3982.

(20) Xu, J.; Li, G.; Li, L. *Mater. Res. Bull.* **2008**, *43*, 990–995.

(21) Lu, Q.; Zeng, H.; Wang, Z.; Cao, X.; Zhang, L. *Nanotechnology* **2006**, *17*, 2098–2104.

(22) Chen, J. S.; Zhu, T.; Li, C. M.; Lou, X. W. *Angew. Chem. Int. Ed.* **2011**, *50*, 650–653.

(23) Schliehe, C.; Juarez, B. H.; Pelletier, M.; Jander, S.; Greshnykh, D.; Nagel, M.; Meyer, A.; Foerster, S.; Kornowski, A.; Klinke, C.; Weller, H. *Science* **2010**, *329*, 550–552.

(24) Oswald, H. R.; Asper, R. In *Preparation and Crystal Growth of Materials with Layered Structures*; Lieth, R. M. A., Ed.; D. Reidel: Dordrecht, The Netherlands, 1977; p 107.

(25) Kolasinski, K. W. *Foundations of Catalysis and Nanoscience*, 2nd ed.; John Wiley and Son: West Sussex, England, 2008; p 236.

(26) Gregg, S. J.; Sing, K. S. W. *Adsorption, Surface Area and Porosity*, 2nd ed.; Academic Press: London, 1982; p 4.

(27) Chen, X.; Shen, Y.-F.; Suib, S. L.; O'Young, C. L. *Chem. Mater.* **2002**, *14*, 940–948.

(28) Chen, C.-H.; Abbas, S. F.; Morey, A.; Sithambaram, S.; Xu, L. P.; Garces, H. F.; Hines, W. A.; Suib, S. L. *Adv. Mater.* **2008**, *20*, 1205–1209.

(29) Xiaobo, F.; Jiyun, F.; Huan, W.; Ka Ming, N. *Catal. Commun.* **2009**, *10*, 1844–1848.

(30) Xiaobo, F.; Jiyun, F.; Huan, W.; Ka Ming, N. *Nanotechnology* **2009**, *20*, 375601.

(31) Pavel, K.; Cecile, D.; Pierre, G.; Michele, B. *Catal. Today* **2007**, *121*, 13–21.

(32) Cecile, D.; Pavel, K.; Pierre, G.; Michele, B. *Appl. Catal., B* **2007**, *70*, 621–629.

(33) Feng, W.; Wataru, U. *Appl. Catal., A* **2008**, *346*, 155–163.

■ NOTE ADDED AFTER ASAP PUBLICATION

An incomplete, early version of this Communication was published ASAP February 18, 2011. The final peer-reviewed and accepted version, with revisions to the text, references, and graphics, was published March 2, 2011.